ACS Sustainable Chemistry & Engineering

pubs.acs.org/journal/ascecg

Research Article

Fabrication of Extremely Concentrated Silver Hydrosols without Additional Stabilizers

Sergey A. Vorobyev,* Maxim N. Likhatski, Alexander S. Romanchenko, Olga Y. Fetisova, Alexander S. Kazachenko, Mikhail N. Volochaev, and Yuri L. Mikhlin*

Cite This: *ACS Sustainable Chem. Eng.* 2020, 8, 17225−17233

Read Online

ACCESS | Metrics & More | Article Recommendations | Supporting Information

ABSTRACT: Applications of silver nanoparticles (Ag NPs) in modern technologies require environmentally friendly methods of large-scale production of the nanoparticles with controlled morphology and surface state in the form of high-concentration metal sols with minimal quantities of organic stabilizers. Herein, we report a procedure based on reduction of aqueous silver nitrate with ferrous sulfate in the presence of citrate ions. We studied the effect of various factors on the chemical reaction by applying transmission electron microscopy, ultraviolet−visible absorption spectroscopy, and dynamic light scattering (DLS) and proposed protocols with reduced quantities of the reagents allowing preparation of uniform spherical Ag NPs of 5 to 15 nm in diameter. A DLS study of sols after dilution was employed to estimate the tendency of colloidal particles to interact in order to optimize post-synthetic purification and concentration procedures. Particularly, filtration instead of centrifugation and electrolytic coagulation with trisodium citrate in place of sodium nitrate were utilized to produce extremely concentrated, more than 1000 g/L Ag, and stable silver hydrosols with no additional stabilizers. The chemical, X-ray photoelectron spectroscopy, and thermogravimetric analyses demonstrated that the Ag NPs contained citrate-derived capping ligands, and low amounts of Fe are appropriated for chemical and low-temperature sintering, surface functionalization, nanofluidics, and other applications.

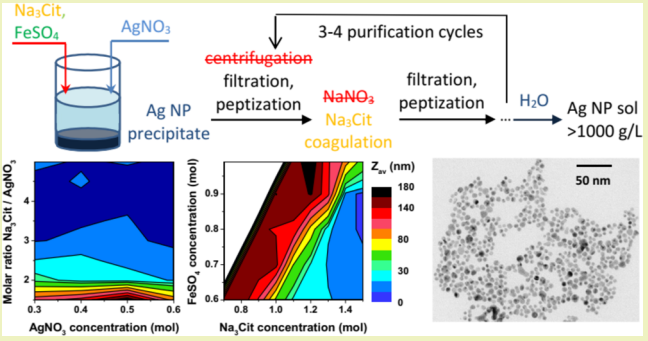

KEYWORDS: *silver nanoparticles, Carey Lea colloid, dense hydrosols, synthesis, dynamic light scattering, hydrophilic surfaces*

INTRODUCTION

Silver nanoparticles are widely used at present in such fields as catalysis, biomedicine, two-dimensional (2D) and 3D printing, optoelectronics, analytics, and many others.[1−7] This requires large-scale manufacturing of the nanoparticles with controllable size, shape, surface capping, and other characteristics by utilizing inexpensive and environmentally friendly reagents. Chemical synthesis of metal nanoparticles in aqueous solutions is a common technique that employs a reducing agent and organic ligands, which prevent aggregation and oxidation of colloidal particles,[1−3] with citrate being one of the most widespread biocompatible reagent, for example.[6,7] The diluted solutions typically allow us to prepare colloids with a concentration of metals on the order of 1 mmol/L, which entails handling and recycling or disposal of large volumes of the spent solutions. Much more concentrated sols needed for a number of applications,[8−22] including inks for printable electronics,[10−15] antibacterial and antifungal materials for agriculture, food industry, healthcare, and textiles,[1,15−20] nanofluids for energetics,[21,22] and so forth, are generally stabilized with large quantities of high-molecular-weight organic compounds, which have to be removed through heating or other methods in order to obtain conductive printed patterns or to be replaced with specific surface functional groups. Production of "dense" metal colloids with a low content of organic stabilizers remains a challenge, although there are examples of commercial, very concentrated hydrosols of silica[23,24] and metal oxides;[25,26] their stability mechanisms, probably beyond the classical Derjaguin−Landau−Verwey−Overbeek (DLVO) model,[27−30] are not understood up to now.

The synthesis of aqueous colloidal solutions of Ag NPs with the concentration as high as 50−150 g/L by means of reduction of aqueous Ag^+ with ferrous ions in the presence of trisodium citrate $Na_3(COO)_3COH(CH_2)_2$ (further denoted as Na_3Cit) at a typical molar ratio $AgNO_3/FeSO_4/Na_3Cit$ of 1:1.8:3.2 followed by several coagulation−peptization steps with alkali metal nitrate has been proposed by Carey Lea[31]

Received: August 16, 2020
Revised: October 1, 2020
Published: November 12, 2020

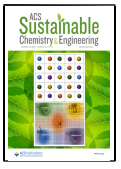

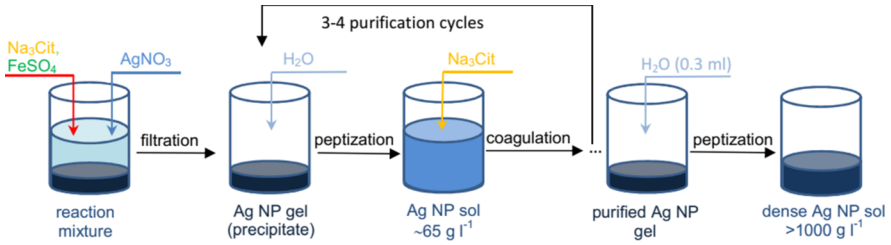

Figure 1. Scheme illustrating the synthesis and purification of Ag NPs via filtration, coagulation with 0.4 M trisodium citrate solution, and peptization in water. The highly concentrated hydrosols are obtained after 3−4 purification steps by dissolving the coagulated precipitate (purified gel) in a small volume of deionized water.

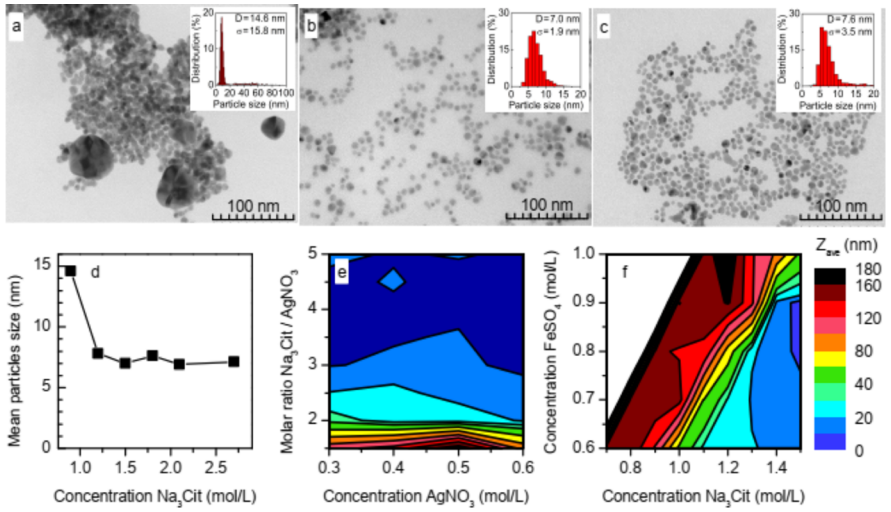

Figure 2. TEM micrographs, particle size distribution histograms (a−c), and (d) dependence of the mean diameter on the initial concentration of trisodium citrate: (a) 0.9 M Na_3Cit, (b) 1.5 M Na_3Cit, and (c) 1.8 M Na_3Cit. 0.6 M $AgNO_3$ and 0.6 M $FeSO_4$; the rate of silver nitrate solution injection of 20 mL/s, an agitation rate of 1000 rpm, and 25 °C. Effect of (e) concentration of $AgNO_3$ and the molar ratio of Na_3Cit to $AgNO_3$ and (f) concentrations of Na_3Cit and $FeSO_4$ on the average hydrodynamic diameter Z_{av} in the Ag NP hydrosols after dilution (1:1000).

more than 130 years ago. However, it has received very limited attention,[32−41] for example, as a medium for SERS,[36,37] because these hydrosols are composed of insufficiently uniform Ag NPs (mainly 6−20 nm spheroids but also larger ones, nanoplates, and rods) contaminated with Fe and are not concentrated enough for many applications. Studies targeted at optimization of characteristics of the colloids are rare; for example, the homogeneous nanoparticles of about 20 nm[38] have been reported to be produced with enhanced concentration of citrate (molar ratio $AgNO_3/FeSO_4/Na_3Cit$ of 1.0:1.8:4.8). It is also worth mentioning the very recent synthesis of a variety of citrate-stabilized nanoparticles of precious metals using iron(II) as a reducing agent.[42] The studies conducted with the Carey Lea colloidal solutions after their dilution have suggested[33−36] that the Ag NPs negatively charged due to citrate anion adsorption obey the DLVO model; the reasons for the unusual stability of the dense sols remain elusive. Recently, we found[39−41] that the species adsorbed on the Ag NP surfaces are actually the products of citrate decomposition comprising an alcohol group and one or two carboxylates, in contrast to three carboxylic groups in citrate anions, and very minor ferric hydroxides. The citrate-derived capping ligands on immobilized Ag NPs can be easily oxidized or replaced in chemical reactions, promoting, in particular, room-temperature sintering of ∼7 nm Ag NPs into submicrometer entities or continuous coatings,[41] promising for flexible electronics, catalysis, and other applications.

The aim of the current research study was to develop methods for manufacturing uniform Ag NPs, improving the purity, and drastically increasing the concentration of silver colloids, by revealing the role of various reaction parameters and post-synthetic procedures. We managed to obtain extremely concentrated Ag hydrosols, whose stability was tentatively attributed to repulsive forces between water layers at hydrophilic particle surfaces in the electrolyte-free aqueous media, but this requires further investigation.

RESULTS AND DISCUSSION

Effect of Reagent Concentrations. Silver nanoparticles produced in the reaction of Ag^+ and Fe^{2+} quickly precipitate in the aqueous medium with the high salt concentrations.[31−41] The sediment was separated with filtration (in the modified method) or centrifugation and dissolved in a portion of water (Figure 1).

This "zero" hydrosol contained about 0.6 mol/L (∼64 g/L) Ag and was diluted for transmission electron microscopy (TEM), dynamic light scattering (DLS), zeta potential, and UV−vis spectroscopy characterization or was purified using several coagulation−filtration (centrifugation)−peptization cycles. The purified residue can be redispersed in a small volume of water yielding a highly concentrated hydrosol. Figure 2 shows representative TEM images (a−c) and the plot of the average diameter of Ag NPs in the "zero" sols (d) as a function of citrate concentration in the initial reaction media.

https://dx.doi.org/10.1021/acssuschemeng.0c06006
ACS Sustainable Chem. Eng. 2020, 8, 17225−17233

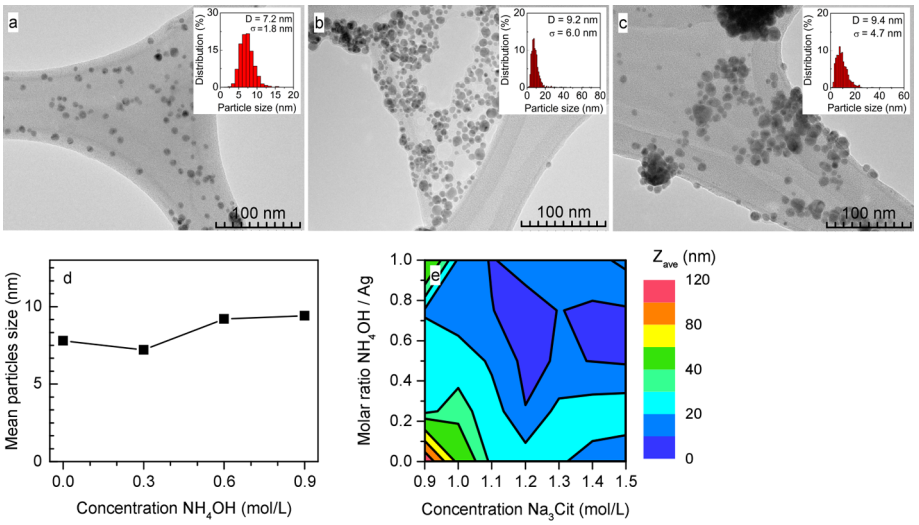

Figure 3. TEM images, particle size distribution histograms for Ag NPs prepared with (a) 0.3 M, (b) 0.6 M, and (c) 0.9 M NH_4OH, and (d) mean diameter of nanoparticles as a function of initial concentrations of ammonia. The reagent concentrations are 0.6 M $AgNO_3$, 0.6 M $FeSO_4$, and 1.2 M Na_3Cit; the rate of silver nitrate solution injection of 20 mL/s, an agitation rate of 1000 rpm, and 25 °C. (e) DLS data on the influence of concentration of Na_3Cit and the molar ratio of NH_4OH to $AgNO_3$ on the average hydrodynamic diameter Z_{av} in the diluted Ag NP hydrosols (1:1000).

The mean particle diameter decreased to about 7 nm with the citrate content approaching 1.2−1.5 mol/L and then stayed almost constant, but the size distribution was narrower and the aggregation was lower for the higher citrate concentrations (additional images are given in Figures S2 and S3, Supporting Information).

The DLS study (Figure 2e,f, see also the Supporting Information) of the Ag hydrosols produced by filtration and dilution of the initial residue in water (data on the dilution 1:1000 are presented) was performed to estimate persisting interactions between the colloidal particles as a function of the reagent concentrations. The dependence of the reaction ratio of citrate-to-silver ions on the average hydrodynamic diameter Z_{av} calculated from cumulant fits of correlation functions[43−46] at various concentrations of silver nitrate is presented in Figure 2e. The size distribution fit of the correlation function[44,45] often showed that the main nanoparticle diameter d_1 concurred with TEM, but it was insufficiently reliable and less informative in terms of particle interactions. The d_1 data acquired in the same experiments as Z_{av} are presented in Figures S4−S8 together with the regressive equations S1−S3 quantifying the effect of various parameters on Z_{av}.

The Z_{av} magnitude rapidly decreased toward the dimensions observed in TEM, suggesting lower aggregation of colloidal particles, as the citrate to Ag ratio approached 2 and then much slower at higher citrate concentrations. Z_{av} reduced with increasing concentration of citrate and decreasing that of ferrous ions (Figure 2f); the initial citrate concentration should be higher than ∼1 mol/L and the molar ratio of citrate to Fe^{2+} larger than 1.5−2 to prepare fine and stable colloidal particles. Aggregation and sedimentation were observed at a ratio less than 1. Zeta potentials of the hydrosols were measured to be in the range −30 to −50 mV.

The effect of concentrations of the reagents (or volume of the solutions added keeping the same quantities) was also studied, and it appeared (Figure S6, Supporting Information) that the concentration of $AgNO_3$ has a small impact, while dilution of the citrate solution is desirable.

These findings appear to indicate that citrate plays the role of both a protective ligand for Ag NPs and a complexing agent for Ag^+ cations;[6,47−49] so, we tested the influence of aqueous ammonia, which has been successfully used in Ag NP syntheses.[8,50−54] It was found (Figure 3, equation S2, Supporting Information) that the citrate content can be reduced down to 1.2 mol/L by adding ammonia to the concentration of 0.3 mol/L to produce Ag NPs of ∼7 nm in diameter, but the particles became coarser and less uniform at higher concentrations. Moreover, the dense hydrosols with ammonia exhibit reduced long-term stability.

We also examine the influence of temperature of the reaction media in the range from −10 to 80 °C (Figure 4, see also Figure S2). The Ag NP diameter and hydrodynamic diameter Z_{av} were lowest, and the particle size and shape were more uniform at the temperature slightly above 0 °C and worse at enhanced temperatures.

So, the concentrations of aqueous $AgNO_3$ of 0.6 mol/L, sodium citrate of 1.2−1.5 mol/L, ferrous sulfate of 0.6−0.8 mol/L without ammonia, or 0.6, 0.9, and 0.6 mol/L, respectively, with 0.3 mol/L NH_4OH and the temperature of 20 °C or lower can be recommended as optimal conditions for the synthetic reaction. The rates of injection of $AgNO_3$ solution and agitation of the reaction medium (Figure S7, Supporting Information) should be large enough, e.g., 20 mL/s and 1000 rpm, respectively.

Purification of the Carey Lea Ag NPs. Tuning the reaction conditions allowed us to reduce the quantities of reagents by about two times, with the ratio of $AgNO_3/FeSO_4/Na_3Cit$ changed from 1.0:1.8:3.2 for the classical formulation to 1.0:1.0:1.5 for the modified one, and to prepare more uniform Ag NPs. However, an electrolyte, typically 1 M $NaNO_3$ solution, had to be added in order to purify the Carey Lea hydrosol via a few cycles of coagulation, centrifugation discarding the supernatant, and redispersion of the residue in water.[31−41] Figure 5 shows that the hydrodynamic diameter Z_{av} of the Ag colloids increased after repeating the coagulation−centrifugation−peptization cycle, possibly due to partial removal of protecting ligands (see Figure S8 for the

https://dx.doi.org/10.1021/acssuschemeng.0c06006
ACS Sustainable Chem. Eng. 2020, 8, 17225−17233

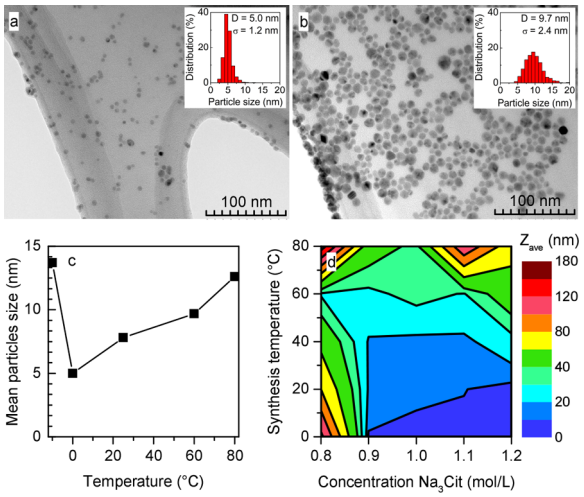

Figure 4. TEM images, particle size distribution histograms, at various reaction temperatures of (a) 0 °C and (b) 60 °C, and (c) mean diameter as a function of temperature of the synthesis with 0.6 M $AgNO_3$, 0.6 M $FeSO_4$, and 1.2 M Na_3Cit (the rates of silver nitrate solution injection and agitation were 20 mL/s and 1000 rpm, respectively). (d) Average hydrodynamic diameter Z_{av} (dilution 1:1000) as a function of temperature at various initial concentrations of trisodium citrate.

corresponding d_1 data). Aging the residue and high centrifuge acceleration resulted in some increase in the Z_{av} magnitude too, suggesting that particle interactions arise in the precipitates (gels). On the other hand, the supernatants (from reaction solution and, in a lesser extent, coagulation electrolyte) were incompletely separated at low centrifugation rates as it is seen from the conductivities of the hydrosol (Figure 5c). The findings indicate that it is necessary to avoid excessive thickening of the precipitates, especially in the first phase separation, whereas the high centrifuge acceleration was not very efficient in removal of electrolyte ions. The increase in the initial citrate concentration promoted the colloidal stability over the purification.

Consequently, we chose filtration for separating the precipitate from remaining reagents in the aqueous reaction media and from the electrolyte in the purification and trisodium citrate as the coagulant (usually 0.4 mol/L) instead of sodium (or potassium) nitrate. Citrate acts also as a complexing agent for Fe[54,55] that was expected to facilitate its dissolution and removal. Figure 6 compares the representative TEM images (a,b) and other sol characteristics for the traditional and optimized methods. Conductivities of hydrosols (Figure 6c) obtained using the new filtration-assisted method (plot 1) are substantially lower than those involving centrifugation, both with $NaNO_3$ and Na_3Cit as coagulants (plots 2 and 3). UV−vis spectra (Figure 6d) exhibit a narrower localized surface plasmon resonance peak at ∼400 nm and negligible absorbance at higher wavelengths, which are due mainly to particle aggregation, as it follows from the DLS and TEM data. Noteworthy, the longwave intensity and then aggregation are larger for centrifugation than filtration with a trisodium citrate coagulant but lower than with sodium nitrate.

Finally, Figure 6e demonstrates that the concentration of Fe decreased from about 5 g/L in the "zero" hydrosol down to 0.25 g/L, while the Ag content slightly enhanced from 64 g/L over the purification with the same volume portions of the coagulant solution. After the third or fourth step, the filtration residue can be dissolved in a very small amount of deionized water (Figure 1), e.g., 0.3 mL, yielding extremely concentrated, 1100 g/L Ag, silver colloids stable for several weeks at least. In effect, concentrations of Ag as high as 1500 g/L can be reached using an appropriate water volume for peptization. At higher Ag concentrations, the colloids separated into a dark precipitate (gel) and a light supernatant. This gel and even the residue dried in air can be easily redispersed in an additional quantity of water to form a less concentrated sol.

Characterization of Ag NPs. X-ray photoelectron spectra (XPS) of dried hydrosols (Figure 7) show that surface concentrations of Na, Fe, and O relative to Ag are lower for the Ag NPs prepared using the modified method in comparison with the traditional Carey Lea technique, with the atomic Ag/Fe ratio being at least ∼40 (the main Ag and Fe lines overlap making precise calculations difficult). The binding energy (BE) of the Ag $3d_{5/2}$ peak of 368.3 eV and the kinetic energy of Ag $M_4N_{45}N_{45}$ maximum at 357.9 eV are characteristic of elemental silver, although insignificant broadening and asymmetry, larger for the classical Carey Lea particles, may suggest the presence of very minor oxidized silver, possibly as surface Ag_2O (367.7 eV) and aqueous Ag^+ species (369 eV).[39−41,56−58] The C 1s spectra depict, apart from the signals from the HOPG support (284.5 eV) and aliphatic carbon, largely from surface contaminations (285−285.4 eV), the lines of an alcoholic group (286.5 eV) and carboxylic species bounded with Ag (288.2 eV) and unbounded (289 eV) of citrate-derived ligands.[39−41] For both particle types, the proportion of carboxylic to alcoholic groups is about 1.2−1.5

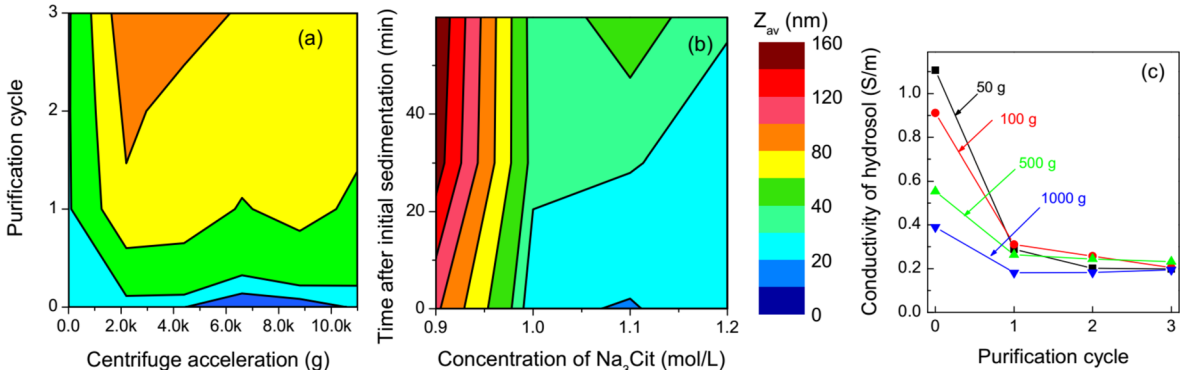

Figure 5. Effect of parameters of purification of Ag NPs through coagulation with 1 M $NaNO_3$ and centrifuge acceleration on Z_{av} (a,b) and on (c) sol conductivity. Reaction conditions: 0.6 M $AgNO_3$, 0.6 M $FeSO_4$, 1.2 M Na_3Cit, and 0 °C; centrifuge accelerations are marked in the plot (c).

https://dx.doi.org/10.1021/acssuschemeng.0c06006
ACS Sustainable Chem. Eng. 2020, 8, 17225−17233

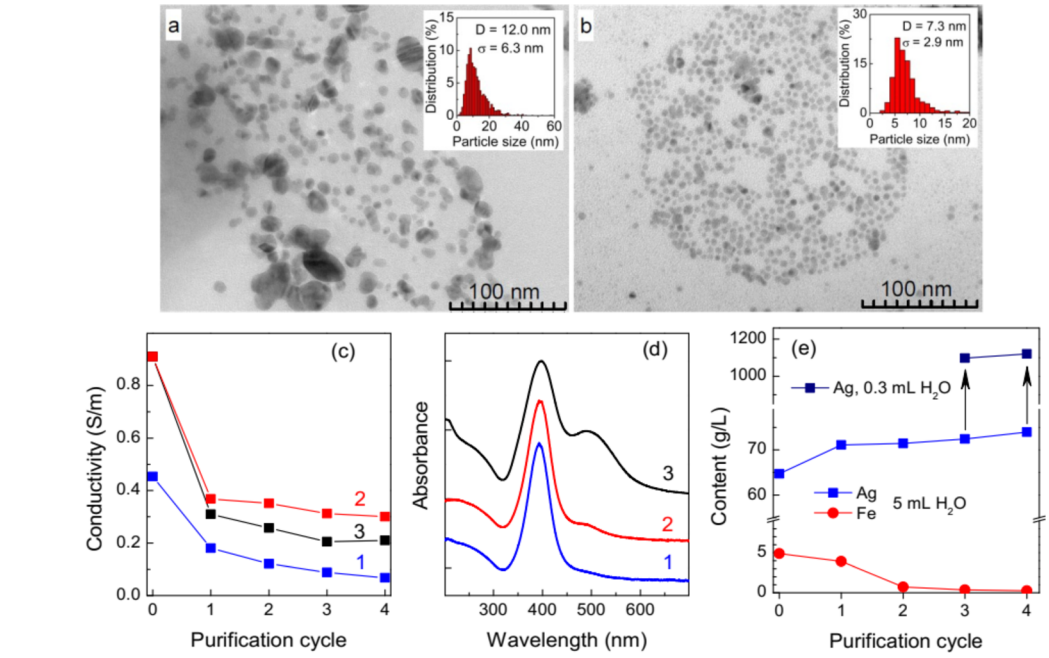

Figure 6. TEM images of Ag NPs prepared with the technique involving (a) centrifugation and 1 M $NaNO_3$ and (b) new method with filtration and 0.4 M Na_3Cit as a coagulant. (c) Conductivity and (d) UV−vis absorption spectra of Ag NP hydrosols produced using (1) filtration and coagulation with 0.4 M Na_3Cit, (2) centrifugation and coagulation with 0.4 M Na_3Cit, and (3) centrifugation and coagulation with 1 M $NaNO_3$. (e) Changes of concentrations of Ag and Fe in hydrosols prepared through the novel synthesis method with filtration and trisodium citrate (0.4 mol/L) coagulation. Concentrations of Ag in the colloids obtained by peptization of the third and fourth filtration residues in a small water volume (0.3 mL instead of 5 mL) are pointed by arrows. Reaction conditions: 0.6 M $AgNO_3$, 0.6 M $FeSO_4$, 1.2 M Na_3Cit, and 0 °C.

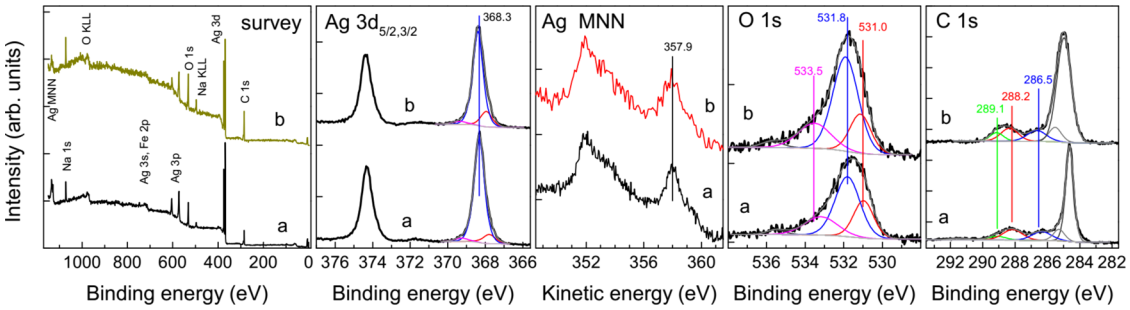

Figure 7. X-ray photoelectron spectra of the Ag NPs prepared with (a) 0.6 M $AgNO_3$, 0.6 M $FeSO_4$, and 1.2 M Na_3Cit (modified method) and (b) 0.6 M $AgNO_3$, 1.8 M $FeSO_4$, and 3.2 M Na_3Cit (Carey Lea method).

that is notably lower than 3:1 in citrate, which appears to decompose on the Ag surface upon the preparation. The O 1s spectra are mainly due to citrate-related species and adsorbed water (Figure 7). The XPS spectra also show that the moderate negative charge of Ag NPs is due to (unbounded) carboxylate groups and suggest a hydrophilic character of the surface. In more detail, the XPS results on the state of Carey Lea nanoparticle surfaces were reported and discussed elsewhere.[40]

Thermogravimetric and differential scanning calorimetry analysis (Figure 8) found larger total weight losses for the nanoparticles produced with the traditional Carey Lea than for the new one (8.8% vs. 2.8%). The heating in an inert atmosphere involves evaporation of water (about 1 and 0.5%, respectively); two reactions at 200 and 350 °C, which are due to decomposition of the citrate-derived organic matter,[59,60] are much smaller, shifted to higher temperatures, and are slightly exothermic, probably owing to the effect of an oxygen-bearing Ag surface, than the reactions of trisodium citrate. The endothermic weight loss at the temperatures higher than 650 °C (less than 0.5% of total mass for the modified Ag NPs) seems to be due to decomposition of impurities of Fe and Na salts. The results demonstrate that the Ag NPs immobilized from the highly concentrated hydrosols contained very minor quantities of bounded water and organic and mineral contaminations, making them suitable for many applications even in comparison to the traditional Carey Lea NPs, which can easily enter various reactions.[39,41]

The very high concentration and stability of hydrosols (let us reiterate that the silver concentrations reached were about 100 and >1000 g/L in the classical Carey Lea method and the modified one, respectively) are likely related with low residual concentrations of electrolyte ions. It should be noted that the dense hydrosols of silica commercially produced since 1950s are based on the seminal work of P.G. Bird who proposed to remove alkali metal ions and other electrolytes by ion exchange or sorption "as far as possible".[23] The very concentrated aqueous colloids have been reported to form also in bimodal systems of silica and metal oxide nanoparticles.[28−30] Up to

https://dx.doi.org/10.1021/acssuschemeng.0c06006
ACS Sustainable Chem. Eng. 2020, 8, 17225−17233

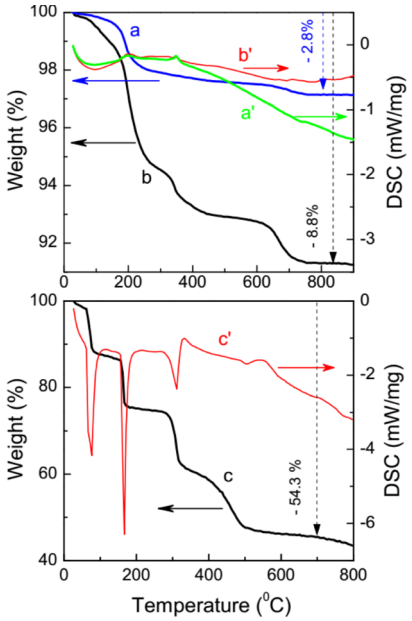

Figure 8. TG (a−c) and DSC (a′−c′) profiles for Ag NPs prepared with (a,a′) 0.6 M $AgNO_3$, 0.6 M $FeSO_4$, and 1.2 M Na_3Cit (modified method) and (b,b′) 0.6 M $AgNO_3$, 1.8 M $FeSO_4$, and 3.2 M Na_3Cit (traditional Carey Lea method) and predried in air, in comparison with (c,c′) trisodium citrate pentahydrate heated in an Ar atmosphere.

now, the mechanisms behind unique aggregative stability of such colloids are questionable. We hypothesize that the phenomena can be related to repulsive hydrophilic forces[27,61−63] between water layers on the nanoparticles, which are still poorly studied and require much more attention; the problem, however, is beyond the scope of the current article.

The above synthesis protocol and general strategy can be utilized for large-scale green production of Ag NPs and probably other metal and metal compound nanoparticles. Citrate-derived capping ligands can be easily replaced with different species, which are required to functionalize the metal particle surface or to form new chemical compounds. For instance, we demonstrated[41] that the immobilized Ag NPs enter diverse room-temperature chemical sintering reactions with aqueous complexes of precious metals, oxidants, and sulfide ions. The very dense hydrosols of Ag NPs are prospective for their usage as inks, antimicrobials, nanofluids, etc. Furthermore, easy availability of such concentrated stabilizer-free fluid metal dispersions opens a way to novel applications and (nano)technologies.

CONCLUSIONS

The effect of various factors on the chemical reduction of Ag nitrate with ferrous sulfate in the presence of citrate ions (Carey Lea method) was studied by applying DLS, zeta potential, TEM, UV−vis absorption spectroscopy, XPS, and TG/DTA, and the results were used in order to optimize the reaction conditions and post-synthetic procedures. Particularly, a DLS study of sols after dilution was used to estimate the tendency of colloidal particles to interact and aggregate by analyzing the average hydrodynamic diameter Z_{av} determined using the cumulant fit. It was found that the quantities of reagents can be reduced to the molecular ratios $AgNO_3$/$FeSO_4$/Na_3Cit of 1:1:2, and the relative concentration of citrate can be further decreased to 1.5 if aqueous ammonia was added. More uniform and less aggregated Ag NPs formed at reduced reaction temperatures and under high speeds of agitation and injection of $AgNO_3$ solution. Examination of the sol purification via electrolytic coagulation of the Ag NPs and centrifugation revealed that the particle interaction increased with the cycle number and centrifuge acceleration, probably due to depletion in the amount of protective ligands and excessive thickening of the precipitate, and with increasing the concentration of the residual electrolyte. To tackle the problem, we used filtration instead of centrifugation and replaced $NaNO_3$ with trisodium citrate in the electrolytic coagulation. This allowed obtaining extremely concentrated, more than 1000 g/L, and stable silver hydrosols with no additional stabilizers. The chemical, XPS, and thermogravimetric analyses found less than 3 wt % impurities (surface ligands, water, Fe, and Na) in the Ag NPs desiccated in ambient air. The mechanism of unusual sol stability may be tentatively attributed to hydrophilic surface forces in the electrolyte-free aqueous media, but further exploration is required. The strategy can be utilized for large-scale production of nanoparticles of Ag and probably other substances as very dense hydrosols for the application as inks, antimicrobials, nanofluids, and others; the findings can also pave the way for novel materials and technologies.

EXPERIMENTAL SECTION

Materials and Preparation Methods. Silver nitrate ($AgNO_3$), iron sulfate ($FeSO_4·7H_2O$), trisodium citrate ($Na_3Cit·5.5H_2O$), sodium nitrate ($NaNO_3$), and aqueous ammonium ($NH_3·H_2O$) were of analytical grade and used as received. Deionized water (Millipore Milli-Q grade) was utilized to prepare all the solutions, to redisperse Ag NPs, and to rinse the samples deposited onto substrates.

The synthesis of silver nanoparticles was carried out according to the original (in fact, slightly adapted) Carey Lea method[31] and the modified technique at varied concentrations of reagents, temperature, and injection and agitation rates using a homemade experimental setup (Figure S1, Supporting Information) constructed of a solution injection block driven by a Nema 23HS5628 and a reaction cell stirred with Nema 17HS2408 stepper motors controlled with Arduino Nano 3.0 and domestic software and thermostatic with a FT-211-25 cryothermostat (LOIP, Russia). In a typical experiment, 5 mL of Na_3Cit solution (0.7−2.7 mol/L), 5 mL of $FeSO_4$ (0.6−1.0 mol/L) fresh solution, and 0.0−0.25 mL of NH_4OH solution (12 mol/L) were loaded in the reaction cell and agitated with a magnetic stirrer (100−1200 rpm) for 5 min at a desired temperature (−10 to 80 °C). Then, $AgNO_3$ solution (0.6 mol/L, 5 mL) was injected with the rate of 1.0−20.0 mL/s, and the reaction media were stirred for another 5 min; a black silver residue was formed almost immediately after mixing the reagent solutions.

The reaction product was centrifuged for 10 min (CR4000, Centurion Scientific, UK), the precipitate was redispersed in water (5 mL) forming a dark-brown hydrosol, and then, 1 mol/L $NaNO_3$ solution (5 mL) was added to coagulate Ag NPs. The procedure was reproduced two or three times, and the last precipitate was suspended in deionized water ("classical" Carey Lea hydrosol). In the modified method, the Ag suspensions were, in contrast, filtered through a hydrophilic PTFE filter membrane (Lab Supplies, China) or a nylon membrane (Phenomenex, USA) with the pore size of 0.45 μm to separate the nanoparticle sediment from the electrolyte. Then, the Ag NP residue was peptized in deionized water forming the "zero" hydrosol with Ag concentration about 64 g/L. Aqueous solution of Na_3Cit (0.4 mol/L, 5 mL) was used as a coagulant, and the residue formed was filtered and peptized in water (5 mL); the purification was repeated three times. The experiments with centrifugation were performed for comparison too. To prepare highly concentrated, up to

https://dx.doi.org/10.1021/acssuschemeng.0c06006
ACS Sustainable Chem. Eng. 2020, 8, 17225−17233

1500 g/L, silver hydrosols, a minimal volume of water (e.g., 0.2 or 0.3 mL) was added to the residue obtained in the third or fourth purification stage. The colloids prepared without ammonia were stable for an indefinite time; sol−gel transition occurred due to sol centrifugation, evaporation of water, or addition of the electrolyte, where the gels formed could be usually peptized again with a small amount of additional water. To determine contents of Ag and Fe, an aliquot of the hydrosol of known volume was weighted before and after drying in air at 50 °C. The residue was dissolved in nitric acid, and the solution was titrated with KSCN to determine Ag^+ or, after sedimentation of Ag as AgCl, with EDTA to determine Fe^{3+}.

Dynamic Light Scattering and Zeta Potential Measurements. DLS studies together with zeta potential and conductivity measurements were performed using a Zetasizer Nano ZS spectrometer (Malvern Instruments Ltd.) at a scattering angle of 173° in a polycarbonate cell with Pd electrodes, typically at 25 °C. Concentrations of the dense colloids were too high for the measurements, and sols were diluted before the experiments; the data presented here were acquired at 1:1000 dilutions, unless otherwise stated. Nevertheless, the correlation functions often revealed notable particle interaction, where the particle dispersion index (Pdi) was commonly between 0.2 and 0.4. The nanoparticle diameter (d_1) determined using the size distribution analysis implemented in Malvern Zetasizer Software (v7.10) showed the main nanoparticle size of 6−12 nm, in reasonable agreement with TEM data, while one or two minor distribution maxima in the range of decades or hundreds of nm were poorly reproducible and showed no clear regularities. At the same time, the average diameter (Z_{av}) found using a cumulant fit[43−45] varied in a wide range but was well reproducible, and it was utilized in the current research study as an arbitrary value characterizing a measure of particle interaction remained in the diluted hydrosols. The magnitude of hydrodynamic diameter Z_{av} is mapped as a function of the synthesis parameters in order to visualize their effect on the colloid behavior. The role of various factors was also quantitatively calculated with Z_{av} as the target parameter and process conditions as independent variables using Statgraphics Centurion XVI, Design of Experiment (DOE) unit software[64] (see the Supporting Information). The results for each map are based on 244 experimental points measured in 3 parallels.

Characterization Techniques. An HT7700 (Hitachi) transmission electron microscope operating at 110 kV was used for TEM characterization of the hydrosol samples. A droplet of the diluted sol was placed on a carbon-coated copper grid and allowed to dry at room temperature. The particle size distribution was estimated from micrographs for 1500−2000 particles using the ImageJ program.

UV−vis absorption spectra from diluted silver hydrosols were collected in the range 200−800 nm in a thermostatic quartz cell with the optical path of 1 cm by employing a Shimadzu UV 3600 instrument.

X-ray photoelectron spectra were acquired with a SPECS spectrometer (SPECS GmbH) equipped with a PHOIBOS 150 MCD-9 analyzer using monochromatic Al Kα irradiation (1486.6 eV) for excitation. Samples for XPS were prepared by drying a sol droplet on highly oriented pyrolytic graphite (HOPG); the C 1s peak at 284.45 eV from the HOPG substrate was used as a reference. The pressure in an analytical chamber was in the range of 10^{-9} mbar. The C 1s, O 1s, and Ag 3d spectra were fitted using Gaussian−Lorentzian peak profiles after Shirley-type background subtraction by employing CasaXPS software.

Ag NPs for thermogravimetric and differential thermal analysis (TG/DTA) were prepared by desiccating the dense hydrosols in air at room temperature. TG/DTA studies were performed in the range from ambient temperature to 1000 °C using an STA449 F1 Jupiter instrument (Netzsch) at a heating rate of 10 °C/min in argon at a gas flow rate of 50 mL/min.

■ ASSOCIATED CONTENT

Supporting Information

The Supporting Information is available free of charge at https://pubs.acs.org/doi/10.1021/acssuschemeng.0c06006.

Photos of the experimental setup and dense Ag hydrosol, additional TEM images, and DLS data (alternatively processed using size distribution analysis and the regression models on the effect of various parameters on Z_{av}) (PDF)

■ AUTHOR INFORMATION

Corresponding Authors

Sergey A. Vorobyev − *Institute of Chemistry and Chemical Technology, Krasnoyarsk Science Center of the Siberian Branch of the Russian Academy of Sciences, Krasnoyarsk 660036, Russia*; Email: yekspatz@yandex.ru

Yuri L. Mikhlin − *Institute of Chemistry and Chemical Technology, Krasnoyarsk Science Center of the Siberian Branch of the Russian Academy of Sciences, Krasnoyarsk 660036, Russia*; orcid.org/0000-0003-1801-0947; Email: yumikh@icct.ru

Authors

Maxim N. Likhatski − *Institute of Chemistry and Chemical Technology, Krasnoyarsk Science Center of the Siberian Branch of the Russian Academy of Sciences, Krasnoyarsk 660036, Russia*

Alexander S. Romanchenko − *Institute of Chemistry and Chemical Technology, Krasnoyarsk Science Center of the Siberian Branch of the Russian Academy of Sciences, Krasnoyarsk 660036, Russia*

Olga Y. Fetisova − *Institute of Chemistry and Chemical Technology, Krasnoyarsk Science Center of the Siberian Branch of the Russian Academy of Sciences, Krasnoyarsk 660036, Russia*

Alexander S. Kazachenko − *Institute of Chemistry and Chemical Technology, Krasnoyarsk Science Center of the Siberian Branch of the Russian Academy of Sciences, Krasnoyarsk 660036, Russia*

Mikhail N. Volochaev − *Kirensky Institute of Physics, Krasnoyarsk Science Center of the Siberian Branch of the Russian Academy of Sciences, Krasnoyarsk 660036, Russia; Reshetnev Siberian State University of Science and Technology, Krasnoyarsk 660037, Russia*

Complete contact information is available at: https://pubs.acs.org/10.1021/acssuschemeng.0c06006

Author Contributions

The manuscript was written through contributions of all authors. All authors have given approval to the final version of the manuscript.

Notes

The authors declare no competing financial interest.

■ ACKNOWLEDGMENTS

This research was supported by the Russian Science Foundation, grant 18-73-00142 (S.A.V.). We acknowledge that facilities of the Krasnoyarsk Regional Research Equipment Centre of SB RAS were employed in the work.

REFERENCES

(1) *Silver Nanoparticle Applications in the Fabrication and Design of Medical and Biosensing Devices;* Alarcon, E. I., Griffith, M., Udekwu, K. I., Eds.; Springer International Publishing: Switzerland, 2015.

(2) *Silver Nanoparticles. Fabrication, Characterization and Applications*; Khan, M., Ed.; IntechOpen: London, 2018.

(3) Krutyakov, Y. A.; Kudrinskiy, A. A.; Olenin, A. Y.; Lisichkin, G. V. Synthesis and Properties of Silver Nanoparticles: Advances and Prospects. *Russ. Chem. Rev.* **2008**, *77*, 233−257.

(4) Calderón-Jiménez, B.; Johnson, M. E.; Bustos, A. R. M.; Murphy, K. E.; Winchester, M. R.; Baudrit, J. R. V. Silver Nanoparticles: Technological Advances, Societal Impacts, and Metrological Challenges. *Front. Chem.* **2017**, *5*, 1−26.

(5) Da Silva, R. R.; Yang, M.; Choi, S.-I.; Chi, M.; Luo, M.; Zhang, C.; Li, Z.-Y.; Camargo, P. H. C.; Ribeiro, S. J. L.; Xia, Y. Facile Synthesis of Sub-20 nm Silver Nanowires through a Bromide-Mediated Polyol Method. *ACS Nano* **2016**, *10*, 7892−7900.

(6) Pillai, Z. S.; Kamat, P. V. What Factors Control the Size and Shape of Silver Nanoparticles in the Citrate Ion Reduction Method? *J. Phys. Chem. B* **2004**, *108*, 945−951.

(7) Bastús, N. G.; Merkoçi, F.; Piella, J.; Puntes, V. Synthesis of Highly Monodisperse Citrate-Stabilized Silver Nanoparticles of up to 200 nm: Kinetic Control and Catalytic Properties. *Chem. Mater.* **2014**, *26*, 2836−2846.

(8) Kumar, A.; Aerry, S.; Goia, D. V. Preparation of Concentrated Stable Dispersions of Uniform Ag Nanoparticles Using Resorcinol as Reductant. *J. Colloid Interface Sci.* **2016**, *470*, 196−203.

(9) Katiyar, N. K.; Biswas, K.; Tiwary, C. S.; Machado, L. D.; Gupta, R. K. Stabilization of Highly Concentrated Colloidal Suspension of Pristine Metallic Nanoparticles. *Langmuir* **2019**, *35*, 2668−2673.

(10) Bulavchenko, A. I.; Arymbaeva, A. T.; Demidova, M. G.; Popovetskiy, P. S.; Plyusnin, P. E.; Bulavchenko, O. A. Synthesis and Concentration of Organosols of Silver Nanoparticles Stabilized by AOT: Emulsion vs Microemulsion. *Langmuir* **2018**, *34*, 2815−2822.

(11) Black, K.; Singh, J.; Mehta, D.; Sung, S.; Sutcliffe, C. J.; Chalker, P. R. Silver Ink Formulations for Sinter-free Printing of Conductive Films. *Sci. Rep.* **2016**, *6*, 20814.

(12) Kamyshny, A.; Magdassi, S. Conductive Nanomaterials for 2D and 3D Printed Flexible Electronics. *Chem. Soc. Rev.* **2019**, *48*, 1712−1740.

(13) Nayak, L.; Mohanty, S.; Nayak, S. K.; Ramadoss, A. A Review on Inkjet Printing of Nanoparticle Inks for Flexible Electronics. *J. Mater. Chem. C* **2019**, *7*, 8771−8795.

(14) Liao, Y.; Zhang, R.; Qian, J. Printed Electronics Based on Inorganic Conductive Nanomaterials and their Applications in Intelligent Food Packaging. *RSC Adv.* **2019**, *9*, 29154−29172.

(15) Tian, B.; Yao, W.; Zeng, P.; Li, X.; Wang, H.; Liu, L.; Feng, Y.; Luo, C.; Wu, W. All-Printed, Low-Cost, Tunable Sensing Range Strain Sensors Based on Ag Nanodendrite Conductive Inks for Wearable Electronics. *J. Mater. Chem. C* **2019**, *7*, 809−818.

(16) Burduşel, A.-C.; Gherasim, O.; Grumezescu, A. M.; Mogoantă, L.; Ficai, A.; Andronescu, E. Biomedical Applications of Silver Nanoparticles: An Up-to-Date Overview. *Nanomaterials* **2018**, *8*, 681.

(17) Paladini, F.; Pollini, M. Antimicrobial Silver Nanoparticles for Wound Healing Application: Progress and Future Trends. *Materials* **2019**, *12*, 2540.

(18) Lee, S.; Jun, B.-H. Silver Nanoparticles: Synthesis and Application for Nanomedicine. *Int. J. Mol. Sci.* **2019**, *20*, 865.

(19) Sánchez-López, E.; Gomes, D.; Esteruelas, G.; Bonilla, L.; Lopez-Machado, A. L.; Galindo, R.; Cano, A.; Espina, M.; Ettcheto, M.; Camins, A.; Silva, A. M.; Durazzo, A.; Santini, A.; Garcia, M. L.; Souto, E. B. Metal-Based Nanoparticles as Antimicrobial Agents: An Overview. *Nanomaterials* **2020**, *10*, 292.

(20) Yan, A.; Chen, Z. Impacts of Silver Nanoparticles on Plants: A Focus on the Phytotoxicity and Underlying Mechanism. *Int. J. Mol. Sci.* **2019**, *20*, 1003.

(21) Asirvatham, L. G.; Nimmagadda, R.; Wongwises, S. Heat Transfer Performance of Screen Mesh Wick Heat Pipes Using Silver−Water Nanofluid. *Int. J. Heat Mass Transfer* **2013**, *60*, 201−209.

(22) Abdelrazik, A. S.; Al-Sulaiman, F. A.; Saidur, R. Optical Behavior of a Water/Silver Nanofluid and their Influence on the Performance of a Photovoltaic-Thermal Collector. *Sol. Energy Mater. Sol. Cells* **2019**, *201*, 110054.

(23) Bird, P. G. Colloidal Solutions of Inorganic Oxides. *Patent USA* 2 244 325A, June 3, 1941. https://patents.google.com/patent/US2244325A/en.

(24) Deželić, G.; Kratohvil, J. P. Determination of Size of Small Particles by Light Scattering Experiments on Ludox Colloidal Silica. *Kolloid Zeitschrift.* **1960**, *173*, 38−48.

(25) Pavlova-Verevkina, O. B.; Ozerina, L. A.; Chemseddine, A.; Ozerin, A. N. Slow Aggregation and Disaggregation of TiO_2 Nanocrystals in Aqueous HCl Solutions. *J. Sol-Gel Sci. Technol.* **2012**, *63*, 162−167.

(26) Wang, Z.; Feng, P.; Chen, H.; Yu, Q. Photocatalytic Performance and Dispersion Stability of Nanodispersed TiO_2 Hydrosol in Electrolyte Solutions with Different Cations. *J. Environ. Sci.* **2020**, *88*, 59−71.

(27) Grasso, D.; Subramaniam, K.; Butkus, M.; Strevett, K.; Bergendahl, J. A Review of Non-DLVO Interactions in Environmental Colloidal Systems. *Rev. Environ. Sci. BioTechnol.* **2002**, *1*, 17−38.

(28) Zhang, F.; Long, G. G.; Jemian, P. R.; Ilavsky, J.; Milam, V. T.; Lewis, J. A. Quantitative Measurement of Nanoparticle Halo Formation around Colloidal Microspheres in Binary Mixtures. *Langmuir* **2008**, *24*, 6504−6508.

(29) Herman, D.; Walz, J. Y. Effects of Metal Oxide Nanoparticles on the Stability of Dispersions of Weakly Charged Colloids. *Langmuir* **2015**, *31*, 4844−4852.

(30) Marino, E.; Balazs, D. M.; Crisp, R. W.; Hermida-Merino, D.; Loi, M. A.; Kodger, T. E.; Schall, P. Controlling Superstructure-Property Relationships via Critical Casimir Assembly of Quantum Dots. *J. Phys. Chem. C* **2019**, *123*, 16495−13457.

(31) Carey Lea, M. On Allotropic Forms of Silver. *Am. J. Sci.* **1889**, *s3-37*, 476−491.

(32) Frens, G.; Overbeek, J. T. G. Carey Lea's colloidal silver. *Kolloid Z. Z. Polym.* **1969**, *233*, 922−929.

(33) Jolivet, J. P.; Gzara, M.; Mazieres, J.; Lefebvre, J. Physicochemical Study of Aggregation in Silver Colloids. *J. Colloid Interface Sci.* **1985**, *107*, 429−441.

(34) Fornasiero, D.; Grieser, F. The Kinetics of Electrolyte Induced Aggregation of Carey Lea Silver Colloids. *J. Colloid Interface Sci.* **1991**, *141*, 168−179.

(35) Dement'eva, O. V.; Mal'kovskii, A. V.; Filippenko, M. A.; Rudoy, V. M. Comparative Study of the Properties of Silver Hydrosols Prepared by "Citrate" and "Citrate−Sulfate" Procedures. *Colloid J.* **2008**, *70*, 561−573.

(36) Siiman, O.; Bumm, L. A.; Callaghan, R.; Blatchford, C. G.; Kerker, M. Surface-Enhanced Raman Scattering by Citrate on Colloidal Silver. *J. Phys. Chem.* **1983**, *87*, 1014−1023.

(37) Munro, C. H.; Smith, W. E.; Garner, M.; Clarkson, J.; White, P. C. Characterization of the Surface of a Citrate-Reduced Colloid Optimized for Use as a Substrate for Surface-Enhanced Resonance Raman Scattering. *Langmuir* **1995**, *11*, 3712−3720.

(38) Kim, K. Y.; Choi, Y. T.; Seo, D. J.; Park, S. B. Preparation of Silver Colloid and Enhancement of Dispersion Stability in Organic Solvent. *Mater. Chem. Phys.* **2004**, *88*, 377−382.

(39) Mikhlin, Y. L.; Vishnyakova, E. A.; Romanchenko, A. S.; Saikova, S. V.; Likhatski, M. N.; Larichev, Y. V.; Tuzikov, F. V.; Zaikovskii, V. I.; Zharkov, S. M. Oxidation of Ag Nanoparticles in Aqueous Media: Effect of Particle Size and Capping. *Appl. Surf. Sci.* **2014**, *297*, 75−83.

(40) Mikhlin, Y. L.; Vorobyev, S. A.; Saikova, S. V.; Vishnyakova, E. A.; Romanchenko, A. S.; Zharkov, S. M.; Larichev, Y. V. On the Nature of Citrate-Derived Surface Species on Ag Nanoparticles: Insights from X-Ray Photoelectron Spectroscopy. *Appl. Surf. Sci.* **2018**, *427*, 687−694.

(41) Vorobyev, S.; Vishnyakova, E.; Likhatski, M.; Romanchenko, A.; Nemtsev, I.; Mikhlin, Y. Reactivity and Chemical Sintering of Carey Lea Silver Nanoparticles. *Nanomaterials* **2019**, *9*, 1525.

https://dx.doi.org/10.1021/acssuschemeng.0c06006
ACS Sustainable Chem. Eng. 2020, 8, 17225−17233

(42) Fernández-Lodeiro, C.; Fernández-Lodeiro, J.; Carbó-Argibay, E.; Lodeiro, C.; Pérez-Juste, J.; Pastoriza-Santos, I. The Versatility of Fe(II) in the Synthesis of Uniform Citrate-Stabilized Plasmonic Nanoparticles with Tunable Size at Room Temperature. *Nano Res.* **2020**, *13*, 2351−2355.
(43) Carvalho, P. M.; Felício, M. R.; Santos, N. C.; Gonçalves, S.; Domingues, M. M. Application of Light Scattering Techniques to Nanoparticle Characterization and Development. *Front. Chem.* **2018**, *6*, 237.
(44) Cascio, C.; Gilliland, D.; Rossi, F.; Calzolai, L.; Contado, C. Critical Experimental Evaluation of Key Methods to Detect, Size and Quantify Nanoparticulate Silver. *Anal. Chem.* **2014**, *86*, 12143−12151.
(45) Hassan, P. A.; Rana, S.; Verma, G. Making Sense of Brownian Motion: Colloid Characterization by Dynamic Light Scattering. *Langmuir* **2015**, *31*, 3−12.
(46) Bhattacharjee, S. DLS and Zeta Potential − What They are and What They are not? *J. Controlled Release* **2016**, *235*, 337−351.
(47) Henglein, A.; Giersig, M. Formation of Colloidal Silver Nanoparticles: Capping Action of Citrate. *J. Phys. Chem. B* **1999**, *103*, 9533−9539.
(48) Patra, S.; Pandey, A. K.; Sen, D.; Ramagiri, S. V.; Bellare, J. R.; Mazumder, S.; Goswami, A. Redox Decomposition of Silver Citrate Complex in Nanoscale Confinement: An Unusual Mechanism of Formation and Growth of Silver Nanoparticles. *Langmuir* **2014**, *30*, 2460−2469.
(49) Zhang, Q.; Li, N.; Goebl, J.; Lu, Z.; Yin, Y. A Systematic Study of the Synthesis of Silver Nanoplates: Is Citrate a "Magic" Reagent? *J. Am. Chem. Soc.* **2011**, *133*, 18931−18939.
(50) Yin, Y.; Li, Z.-Y.; Zhong, Z.; Gates, B.; Xia, Y.; Venkateswaran, S. Synthesis and Characterization of Stable Aqueous Dispersions of Silver Nanoparticles through the Tollens Process. *J. Mater. Chem.* **2002**, *12*, 522−527.
(51) Gorup, L. F.; Longo, E.; Leite, E. R.; Camargo, E. R. Moderating Effect of Ammonia on Particle Growth and Stability of Quasi-Monodisperse Silver Nanoparticles Synthesized by the Turkevich Method. *J. Colloid Interface Sci.* **2011**, *360*, 355−358.
(52) Montazer, M.; Shamei, A.; Alimohammadi, F. Synthesis of Nanosilver on Polyamide Fabric Using Silver/Ammonia Complex. *Mater. Sci. Eng. C* **2014**, *38*, 170−176.
(53) Buccolieri, A.; Serra, A.; Giancane, G.; Manno, D. Colloidal Solution of Silver Nanoparticles for Label-Free Colorimetric Sensing of Ammonia in Aqueous Solutions. *Beilstein J. Nanotechnol.* **2018**, *9*, 499−507.
(54) Gautier-Luneau, I.; Merle, C.; Phanon, D.; Lebrun, C.; Biaso, F.; Serratrice, G.; Pierre, J.-L. New Trends in the Chemistry of Iron (III) Citrate Complexes: Correlations between X-Ray Structures and Solution Species Probed by Electrospray Mass Spectrometry and Kinetics of Iron Uptake from Citrate by Iron Chelators. *Chem. − Eur. J.* **2005**, *11*, 2207−2219.
(55) Silva, A. M. N.; Kong, X.; Parkin, M. C.; Cammack, R.; Hider, R. C. Iron(III) Citrate Speciation in Aqueous Solution. *Dalton Trans.* **2009**, *40*, 8616−8625.
(56) Kibis, L. S.; Stadnichenko, A. I.; Pajetnov, E. M.; Koscheev, S. V.; Zaykovskii, V. I.; Boronin, A. I. The Investigation of Oxidized Silver Nanoparticles Prepared by Thermal Evaporation and Radio-Frequency Sputtering of Metallic Silver under Oxygen. *Appl. Surf. Sci.* **2010**, *257*, 404−413.
(57) Rocha, T. C. R.; Oestereich, A.; Demidov, D. V.; Hävecker, M.; Zafeiratos, S.; Weinberg, G.; Bukhtiyarov, V. I.; Knop-Gericke, A.; Schlögl, R. The Silver−Oxygen System in Catalysis: New Insights by near Ambient Pressure X-Ray Photoelectron Spectroscopy. *Phys. Chem. Chem. Phys.* **2012**, *14*, 4554−4564.
(58) Ferraria, A. M.; Carapeto, A. P.; do Rego, A. M. B. X-Ray Photoelectron Spectroscopy: Silver Salts Revisited. *Vacuum* **2012**, *86*, 1988−1991.
(59) Gao, J.; Wang, Y.; Hao, H. Investigations on Dehydration Processes of Trisodium Citrate Hydrates. *Front. Chem. Sci. Eng.* **2012**, *6*, 276−281.
(60) Marcilla, A.; Gómez-Siurana, A.; Beltrán, M.; Martínez-Castellanos, I.; Blasco, I.; Berenguer, D. TGA-FTIR Study of the Pyrolysis of Sodium Citrate and its Effect on the Pyrolysis of Tobacco and Tobacco/SBA-15 Mixtures under N_2 and Air Atmospheres. *J. Sci. Food Agric.* **2018**, *98*, 5916−5931.
(61) Lu, L.; Berkowitz, M. L. Hydration Force between Model Hydrophilic Surfaces: Computer Simulations. *J. Chem. Phys.* **2006**, *124*, 101101.
(62) Kanduč, M.; Schlaich, A.; Schneck, E.; Netz, R. R. Water-Mediated Interactions between Hydrophilic and Hydrophobic Surfaces. *Langmuir* **2016**, *32*, 8767−8782.
(63) Kopel, Y.; Giovambattista, N. Comparative Study of Water-Mediated Interactions between Hydrophilic and Hydrophobic Nanoscale Surfaces. *J. Phys. Chem. B* **2019**, *123*, 10814−10824.
(64) Montgomery, D. C.; Runger, G. C.; Hubele, N. F. *Engineering Statistics*; 5th ed., Wiley, 2011, 546

https://dx.doi.org/10.1021/acssuschemeng.0c06006
ACS Sustainable Chem. Eng. 2020, 8, 17225−17233